Available online at www.sciencedirect.com
SCIENCE DIRECT®
Journal of Solid State Chemistry 177 (2004) 2129–2137
JOURNAL OF SOLID STATE CHEMISTRY
http://elsevier.com/locate/jssc

Structure of trihydrated rare-earth acid diphosphates $LnHP_2O_7 \cdot 3H_2O$ (Ln = La, Er)

S. Ben Moussa,[a] S. Ventemillas,[a] A. Cabeza,[b] E. Gutierrez-Puebla,[a] and J. Sanz[a,*]

[a] *Instituto Ciencia de Materiales, CSIC, Cantoblanco, Madrid 28049, Spain*
[b] *Dpto. Quimica, Cristalografia y Mineralogia, Univ. Malaga, Malaga 29071, Spain*

Received 23 July 2003; received in revised form 25 November 2003; accepted 1 February 2004

Abstract

In trihydrated lanthanum acid-diphosphates $LnHP_2O_7 \cdot 3H_2O$, prepared from acid $LnCl_3$ and $Na_4P_2O_7$ solutions (pH = 1), two crystal forms were obtained. Layered structures of two representative members of this family have been determined by single-crystal X-ray diffraction (XRD) technique. In the case of orthorhombic $LaHP_2O_7 \cdot 3H_2O$ (type I), lanthanum cations are ninefold coordinated and diphosphate groups adopt a staggered (alternated) configuration. In the case of triclinic $ErHP_2O_7 \cdot 3H_2O$ (type II), erbium cations are eightfold coordinated and diphosphate groups adopt an eclipsed configuration. In agreement with Infrared (IR) spectroscopic data, a bended configuration for diphosphate groups has been deduced. In both structures, one-dimensional chains of edge-sharing rare-earth polyhedra are linked together by diphosphate groups to form the phosphate layers. In both diphosphates, PO_4 and HPO_4 environments have been identified by ^{31}P MAS-NMR technique. In the two compounds, OH groups of HPO_4 tetrahedra point out of diphosphate planes interacting with adjacent layers. In La-diphosphate, the interaction between HPO_4 groups and water molecules of adjacent layers is favored; however, in Er-diphosphate, the interaction between phosphate acid groups of contiguous layers is produced. Based on structural information deduced, differences detected in IR and NMR spectra of two disphosphates are discussed.

Keywords: Acid diphosphates; Lanthanide series; Single crystals; Lamellar structure; Hydrogen bonds

1. Introduction

Acid orthophosphates with lamellar structure exhibit interesting properties in heterogeneous catalysis [1–4]. In particular, two types of lamellar $Zr(HPO_4)_2$ phosphates have been identified in which adsorption properties depend on hydrogen bond interactions established between contiguous layers [5,6]. During thermal treatment of these compounds, condensation of orthophosphate acid precursors produced diphosphates with interesting mechanical properties [7,8]. In a similar way, tetra, cyclo and polyphosphates with interesting optical properties can be prepared from acid lanthanum diphosphates, depending on the temperature and the time used in thermal treatments [9].

In the case of acid diphosphates of rare-earth trivalent cations, the synthesis has been reported by several authors. $LaHP_2O_7 \cdot 3.5H_2O$ was first described by Tananaev during the investigation of the $La_4(P_2O_7)_3$–$H_4P_2O_7$–H_2O system [10]. In a subsequent work, Kizilyalli described the chemical preparation of $GdHP_2O_7 \cdot nH_2O$ ($n = 3-4$), and its thermal decomposition [9]. Finally, Afonin et al. prepared several $RE^{III}HP_2O_7 \cdot 3.5H_2O$ compounds and identified their corresponding anhydrous phases [11]. In a recent work, in which $RE^{III}HP_2O_7 \cdot 3.5H_2O$ compounds were characterized by X-ray powder diffraction (XPD), infrared (IR) and nuclear magnetic resonance (NMR) techniques [12], two new structural types were identified depending on the radius of rare-earth cations. From La to Sm, diphosphates display the orthorhombic symmetry and from Sm to Yb, diphosphates display the triclinic symmetry [12], the samarium diphosphate being stable in the two polymorphic forms. Structures of $GdHP_2O_7 \cdot 3H_2O$ and $SmHP_2O_7 \cdot 4H_2O$ have been recently reported, showing that the gadolinium compound crystallizes in the previously identified triclinic

*Corresponding author. Fax: +34-913720623.
E-mail address: jsanz@icmm.csic.es (J. Sanz).

0022-4596/$ - see front matter © 2004 Elsevier Inc. All rights reserved.
doi:10.1016/j.jssc.2004.02.002

phase, while the samarium compound displays a new monoclinic phase [13,14].

In order to clarify structural aspects of this family of compounds, crystals of erbium and lanthanum diphosphates have been grown and their crystal structures determined. Erbium compound exhibits the triclinic symmetry and is isostructural to the gadolinium diphosphate previously reported [13]. However, lanthanum diphosphate is orthorhombic and its structure has not been determined. Structural information obtained in two diphosphates has been compared with that deduced by NMR and IR spectroscopies. In particular, information obtained on hydrogen bond interaction between contiguous layers has been used to explain the stretching OH region of IR spectra.

2. Experimental section

2.1. Materials

Rare-earth acid diphosphates were prepared by mixing a sodium diphosphate solution ($Na_4P_2O_7$, 0.1 M) and an acid solution of the rare-earth chloride ($LnCl_3$, 0.1 M) (pH = 1), stirring the resulting solution for 2 h at room temperature. Chemical analysis of diphosphates was carried out with the inductively coupled plasma ICP technique. In all phosphates prepared, the relative amounts of P and *Ln* conform to the molar ratio $Ln/P \approx 1/2$ and the amount of remaining Na and Cl was negligible. From TG and IR data, elimination of water takes place in two stages in the 20–200°C temperature range, and that of OH groups is produced between 200°C and 900°C [12]. The XPD analysis of prepared compounds showed the presence of two different symmetries: $LnHP_2O_7 \cdot 3.5H_2O$, with *Ln* = La–Sm adopted the orthorhombic symmetry but those with *Ln* = Sm–Yb display the triclinic symmetry [12,15].

2.2. Crystal growth

Single crystals of La diphosphate were prepared in a U-tube (2 cm diameter, 17 cm length) double diffusion system, in which a silica hydrogel was formed by adding HCl (1 M) to a $Si(OCH_3)_4$ solution until pH = 5.5. After the gelification process, the silica hydrogel was acidified at pH = 2. The reagents (1 M $LaCl_3$ and 1 M $Na_4P_2O_7$) were then poured in the two separated reservoirs of the U-tube. In order to optimize experimental conditions for the single-crystal growth, a large number of experiments was carried out at 25°C, varying the pH in the range 1–3, the relative reagents concentration and the composition of silica hydrogels. In the case of Er diphosphate, crystals were synthesized in a test tube, where the gel was directly formed in presence of a 1 M $Na_4P_2O_7$ solution. Then, a saturated $ErCl_3$ solution was added into the acidified gel. The nucleation time, associated with the first crystallite detection, was 7 months for La-diphosphate and one week for Er-diphosphate. An inspection of samples under the microscope revealed the presence of small crystallites at the surface of spherical amorphous particles. In each case, several crystallites were removed from these particles for single-crystal determinations.

2.3. Single-crystal XRD analysis. Structure determination

Crystals showing well-defined faces were mounted on a Bruker–Siemens Smart CCD diffractometer equipped with a normal focus, 2.4 kW sealed tube X-ray source (molybdenum radiation, $\lambda = 0.71073$ Å), operating at 50 kV and 30 mA. The crystal detector was positioned 4.52 cm from the sample. More than a hemisphere of the reciprocal space was explored. Each independent exposure (10 s) covered 0.3° of the $2° < \theta < 30°$ region. The first 50 frames were recollected at the end of the data collection to monitor the possible crystal decay.

The cell parameters were determined and refined by least-squares fitting of the strongest reflections [$I > 10\sigma(I)$]. For structural determinations, intensities were corrected for Lorentz and polarization effects. For data collection and data reduction, SMART and SAINT programs (Bruker) were used. Structural analysis was carried out with the SHELXTL (based on SHELXS and SHELXL) software package. Crystal structures were solved by direct methods and difference Fourier synthesis. Refinements were carried out by full-matrix least-squares analysis, using anisotropic thermal parameters for non-hydrogen atoms. In the Erbium diphosphate, the H atoms were located and refined with isotropic thermal parameters. In the Lanthanum diphosphate, the H atoms were fixed at their calculated positions. A summary of crystal refinement data is given in Table 1. Weighted *R* factors (w*R*) and goodness-of-fit parameters are based on F^2, but conventional *R* factors (*R*) are based on *F* structural factors. Further details of the crystal structure determination are provided as supplementary material (see Section 6).

2.4. IR and NMR spectroscopies

For IR spectrometry, samples were diluted with KBr to form pellets (phosphate/KBr ratio = 5% by weight) and examined in the 240 to 4000 cm^{-1} region, using a Nicolet 20 SXC FT-IR spectrophotometer.

^{31}P MAS-NMR spectra of two representative members of prepared diphosphates were recorded at 161.96 MHz using a MSL-400 Bruker spectrometer. For that, La (type I) and Sm (type II) were chosen due to the absence of important paramagnetic interactions.

Table 1
Crystal data and structure refinement parameters for $Ln HP_2O_7 \cdot 3H_2O$ diphosphates.

Empirical form	$LaHP_2O_7 \cdot 3H_2O$	$ErHP_2O_7 \cdot 3H_2O$
Formula weigh	367.91	396.26
Temperature	296(2) K	143(2) K
Wavelength	0.71073 Å	0.71073 Å
Crystal system	Orthorhombic	Triclinic
Space group	*Aba*2	$P\bar{1}$
Unit-cell dimensions	$a = 13.653(2)$ Å, $\alpha = 90°$	$a = 6.3986(5)$ Å, $\alpha = 82.009(2)°$
	$b = 18.526(3)$ Å, $\beta = 90°$	$b = 6.8679(6)$ Å, $\beta = 79.949(2)°$
	$c = 6.8740(10)$ Å, $\gamma = 90°$	$c = 9.7483(8)$ Å, $\gamma = 88.408(2)°$
Volume, Z	1738.7(4) Å^3, 8	417.72(6) Å^3, 2
Density (calculated)	2.811 Mg/m^3	3.150 Mg/m^3
Absorption coefficient	5.314 mm^{-1}	10.461 mm^{-1}
$F(000)$	1392	370
Crystal size	$0.2 \times 0.04 \times 0.04$ mm	$0.02 \times 0.06 \times 0.10$ mm
θ range for data collection	2.66–28.29°	2.14–29.45°
Limiting indices	$-18 \leqslant h \leqslant 6$, $-24 \leqslant k \leqslant 8$, $-8 \leqslant l \leqslant 9$	$-8 \leqslant h \leqslant 7$, $-9 \leqslant k \leqslant 9$, $-13 \leqslant l \leqslant 10$
Reflections collected	3380	2948
Independent reflections	2018 ($R_{int} = 0.0468$)	2035 ($R_{int} = 0.0349$)
Absorption correction	None	None
Refinement method	Full-matrix least-squares on F^2	Full-matrix least-squares on F^2
Data/restraints/parameters	2018/1/118	2035/0/128
Goodness-of-fit on F^2	0.966	0.974
Final R indices [$I > 2\sigma(I)$]	$R_1 = 0.0360$, w$R_2 = 0.0817$	$R_1 = 0.0361$, w$R_2 = 0.0891$
R indices (all data)	$R_1 = 0.0471$, w$R_2 = 0.0852$	$R_1 = 0.0407$, w$R_2 = 0.0922$
Largest diff. peak and hole	2.446 and −1.692 e/Å^3	2.339 and −1.754 e/Å^3

Samples were spun at 4 kHz around an axis inclined 54°44′ with respect to the external magnetic field H_0. MAS spectra were taken after a $\pi/2$ pulse irradiation (6 μs), the number of scans was 20 and the interval between scans 5 s. CP-MAS spectra were obtained by using the Hartman–Hann condition, with a radio-frequency H_{1H} field of 15 G for the decoupler channel (400.13 MHz), and a contact time of 1 ms. Chemical shifts (ppm) were referred to that of an external 85% H_3PO_4 aqueous solution. The analysis of NMR spectra was carried out by using the program WINFIT [16].

3. Results

3.1. X-ray diffraction

3.1.1. Lanthanum diphosphate

An inspection of the sample preparation under the microscope revealed the presence of acicular crystallites at the surface of sphere-shaped particles. The crystallite finally chosen for the structural determinations had $0.2 \times 0.04 \times 0.04$ mm dimensions.

Systematic absences $h\,k\,l$, $k + l = 2n + 1$; $0\,k\,l$, $k = 2n + 1$; $h\,0\,l$, $h = 2n + 1 (l = 2n + 1)$ were detected, that were compatible with *Acam* (#64) or *Aba*2 (#41) space groups. In this work, both solutions were tested, resulting the second structural model chosen during the refinement process. Unit-cell dimensions finally obtained, were $a = 13.653(2)$, $b = 18.526(3)$ and $c = 6.8740(10)$ Å, $V = 1738.7(4)$ Å^3. The final R factor obtained was 0.0360.

Table 2
Atom positions and isotropic thermal factors in $LaHP_2O_7 \cdot 3H_2O$

	X/a	Y/b	Z/c	U_{eq} (Å^2)
La(1)	−0.0722 (1)	0.7086 (1)	0.7332 (2)	0.011 (1)
P(1)	0.1394 (1)	0.5787 (1)	0.7520 (6)	0.015 (5)
P(2)	0.1626 (1)	0.7310 (1)	0.7278 (8)	0.011 (3)
O(1)	0.0357 (4)	0.5993 (3)	0.7970 (8)	0.018 (1)
O(2)	0.1446 (5)	0.5495 (4)	0.5360 (10)	0.025 (2)
O(3)	0.1884 (5)	0.5283 (4)	0.8922 (10)	0.024 (2)
O(4)	0.2066 (4)	0.6506 (3)	0.7530 (17)	0.017 (2)
O(5)	0.0972 (7)	0.7298 (6)	0.5483 (15)	0.014 (2)
O(6)	0.2515 (4)	0.7791 (3)	0.7159 (19)	0.018 (2)
O(7)	0.0943 (8)	0.7444 (7)	0.8996 (16)	0.016 (2)
O(8)	−0.1501 (5)	0.6146 (6)	0.9649 (15)	0.028 (2)
O(9)	−0.1178 (6)	0.6060 (5)	0.4877 (14)	0.028 (2)
O(10)	−0.0505 (5)	0.8540 (3)	0.7200 (30)	0.031 (2)
H(3)	0.2028	0.4885	0.8426	0.050
H(81)	−0.1689	0.5682	0.9849	0.050
H(82)	−0.1849	0.6330	0.9829	0.018
H(91)	−0.1267	0.5609	0.5006	0.037
H(92)	−0.1294	0.6407	0.3400	0.050
H(101)	−0.0376	0.8737	0.8284	0.042
H(102)	−0.0970	0.8702	0.6291	0.013

Structural analysis of this phase showed that the composition of the analyzed crystal was $LaHP_2O_7 \cdot 3H_2O$. Thus, in the unit cell there exist 8 formulas with 1 lanthanum, 2 phosphorous, 7 oxygens and 3 water molecules in the asymmetric unit (see Table 2). Bond

Table 3
Bond lengths (Å) and angles (deg) for $LaHP_2O_7 \cdot 3H_2O$

Tetrahedron P(1)			
P(1)–O(1)	1.499 (6)	P(1)–O(3)	1.498 (7)
P(1)–O(2)	1.582 (8)	P(1)–O(4)	1.617 (5)
		O(3)–H(3)	0.836 (7)
Tetrahedron P(2)			
P(2)–O(4)	1.616 (5)	P(2)–O(6)	1.508 (5)
P(2)–O(5)	1.523 (12)	P(2)–O(7)	1.525 (12)
		P(2)–O(4)–P(1)	123.3 (3)
Polyhedron La			
La–O(1)	2.543 (6)	La–O(7)	2.630 (11)
La–O(5)	2.668 (10)	La–O(7)$^{\#3}$	2.471 (12)
La–O(5)$^{\#2}$	2.472 (11)	La–O(8)	2.589 (9)
La–O(6)$^{\#1}$	2.421 (5)	La–O(9)	2.618 (9)
		La–O(10)	2.711 (6)

Symmetry transformations used to generate equivalent atoms: #1, $x-1/2$, $-y+3/2$, z; #2, $-x$, $-y+3/2$, $z+1/2$; #3, $-x$, $-y+3/2$, $z-1/2$; #4, $x+1/2$, $-y+3/2$, z.

Table 4
Atom positions and isotropic thermal factors in $ErHP_2O_7 \cdot 3H_2O$

	X/a	Y/b	Z/c	U_{eq} (Å^2)
Er(1)	0.3749 (1)	0.2599 (1)	−0.0472 (1)	0.017 (1)
P(1)	0.0554 (3)	0.1433 (3)	0.2879 (2)	0.021 (1)
P(2)	−0.1936 (3)	0.2345 (2)	0.0611 (2)	0.018 (1)
O(1)	0.2433 (8)	0.2370 (7)	0.1889 (5)	0.023 (1)
O(2)	0.0681 (8)	−0.0753 (7)	0.3338 (5)	0.024 (1)
O(3)	0.0090 (9)	0.2606 (8)	0.4148 (6)	0.028 (1)
O(4)	−0.1553 (8)	0.1810 (8)	0.2201 (6)	0.026 (1)
O(5)	−0.3372 (7)	0.4132 (7)	0.0572 (5)	0.019 (1)
O(6)	−0.3289 (8)	0.0707 (7)	0.0310 (5)	0.021 (1)
O(7)	0.0183 (8)	0.2599 (7)	−0.0336 (6)	0.022 (1)
O(8)	0.2928 (9)	0.2599 (9)	−0.2727 (6)	0.029 (1)
O(9)	0.6677 (8)	0.3653 (8)	−0.2325 (6)	0.026 (1)
O(10)[a]	0.4892 (19)	0.6479 (17)	0.5417 (13)	0.034 (2)
O(11)[a]	0.5080 (30)	0.0740 (20)	0.5064 (18)	0.055 (4)
H(3)	−0.014 (18)	0.196 (16)	0.493 (12)	0.05 (3)
H(81)	0.184 (14)	0.198 (13)	−0.279 (9)	0.02 (2)
H(82)	0.361 (15)	0.236 (13)	−0.350 (11)	0.03 (2)

[a] Occupation factors = 1/2.

distances and angles corresponding to this phosphate are given in Table 3. Each lathanum is ninefold coordinated, sharing six oxygens with neighboring lanthanum and phosphorous atoms. Distances La–O are comprised between 2.421(5) and 2.668(10) Å, and La–H_2O between 2.589(9) and 2.711(6) Å. In the case of diphosphate groups, external P–O distances are comprised between 1.498(6) and 1.582(8) Å, P–O distances in P–O–P bridges are 1.617(5) Å and the P–O–P angle is 123.3(3)°.

3.1.2. Erbium diphosphate

The analysis of the second compound under the microscope revealed the presence of small crystallites inside amorphous sphere aglomerates. Some crystallites were tested in single-crystal analysis. The crystallite finally used in these determinations displayed $0.02 \times 0.06 \times 0.1$ mm dimensions.

In $ErHP_2O_7 \cdot 3H_2O$ crystallites the symmetry was triclinic and the space group $P1$ or $P\bar{1}$. The unit-cell parameters are $a = 6.3986(5)$, $b = 6.8679(6)$, $c = 9.7483(8)$ Å, $\alpha = 82.009(2)$, $\beta = 79.949(2)$, $\gamma = 88.408°(2)$, $V = 417.72(6)$ Å^3. The final R factor obtained was 0.0361.

The composition of the analyzed crystal was $ErHP_2O_7 \cdot 3H_2O$. In the unit cell of this phosphate, there are two formulas with 1 erbium, 2 phosphorous, 7 oxygens and 3 water molecules in the asymmetric unit (see Table 4). In this phase, only protons of OH and of one H_2O molecule could be positioned. Bond distances and angles corresponding to this phosphate are given in Table 5. Each erbium is eightfold coordinated, sharing six oxygens with other erbium and phosphorous atoms. Distances Er–O are comprised between 2.241(4) and 2.569(5) Å, and Er–H_2O between 2.348(6) and 2.414(5) Å. In the case of diphosphate groups, external P–O distances are comprised between 1.500(5) and 1.550(6) Å, the P–O distances in P–O–P bridges are 1.602(6) Å, and the P–O–P angle is 132.6(3)°.

Table 5
Bond lengths (Å) and angles (deg) for $ErHP_2O_7 \cdot 3H_2O$

Tetrahedron P(1)			
P(1)–O(1)	1.503 (5)	P(1)–O(3)	1.550 (6)
P(1)–O(2)	1.510 (5)	P(1)–O(4)	1.602 (5)
		O(3)–H(3)	0.82 (11)
Tetrahedron P(2)			
P(2)–O(4)	1.602 (6)	P(2)–O(6)$^{\#5}$	1.528 (5)
P(2)–O(5)$^{\#4}$	1.513 (5)	P(2)–O(7)	1.500 (5)
		P(2)–O(4)–P(1)	132.6 (3)
Polyhedron La			
Er–O(1)	2.293 (5)	Er–O(6)$^{\#3}$	2.440 (5)
Er–O(5)$^{\#1}$	2.241 (4)	Er–O(7)	2.262 (5)
Er–O(5)$^{\#3}$	2.569 (5)	Er–O(8)	2.348 (6)
Er–O(6)$^{\#2}$	2.278 (5)	Er–O(9)	2.414 (5)

Symmetry transformations used to generate equivalent atoms: #1, $-x$, $-y+1$, $-z$; #2, $-x$, $-y$, $-z$; #3, $x+1$, y, z; #4, $-x+1$, $-y$, $-z$; #5, $x-1$, y, z; #6, $-x+1$, $-y$, $-z+1$.

3.2. IR and NMR data

IR spectra of diphosphates described are shown in Fig. 1. Bands in the region 3700–3100 and 1700–1600 cm^{-1} can be attributed to OH/H_2O vibrations and bands below 1300 cm^{-1} to vibrational features of diphosphate groups. In IR spectra of the Sm-diphosphate, the number of intense modes in the range 800–1300 cm^{-1} is higher than in the La-diphosphate,

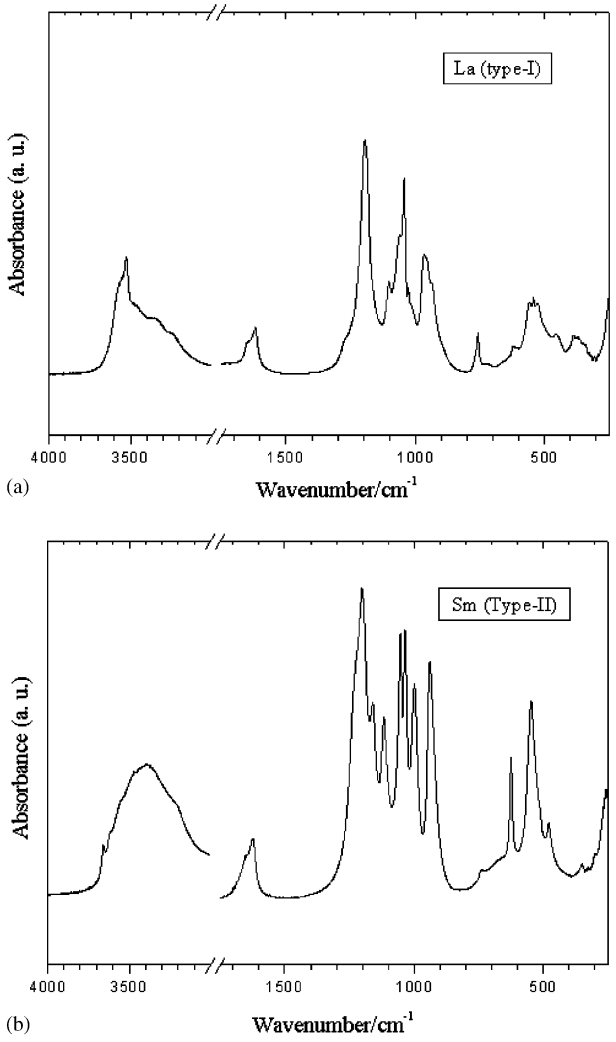

Fig. 1. IR spectra of $LaHP_2O_7 \cdot 3H_2O$ (type-I) (a) and $ErHP_2O_7 \cdot 3H_2O$ (type-II) (b) recorded on samples diluted in KBr pellets.

suggesting that symmetry is different in two compounds [12].

In order to avoid paramagnetic interactions, the analysis of ^{31}P MAS-NMR spectra of rare-earth diphosphates was carried out in La and Sm diphosphates (types I and II). ^{31}P MAS-NMR spectra of analyzed phosphates, Fig. 2, are formed by two components and the corresponding spinning side bands spaced at 25 ppm (spinning rate expressed in cps). In all cases NMR patterns are very broad (150, −150 ppm) indicating that chemical shift anisotropies are more important than P–P or P–H dipolar interactions.

To reduce residual H–P dipolar interactions, CP-MAS experiments were undertaken. In CP-MAS spectra, the component with higher chemical shift narrows and increases its intensity with respect to that located at more negative values. This fact allowed the assignment of both lines to HPO_4 and PO_4 groups respectively. In La diphosphate (type I), both CP-MAS signals have similar intensity; however, in Sm diphosphate (type II) two signals have different intensity, indicating that the cross polarization between protons and P atoms is different (Fig. 2).

4. Discussion

Structural analysis carried out in La and Er diphosphates, shows that the structural formula deduced in both compounds is $LnHP_2O_7 \cdot 3H_2O$. This result indicates that in powder samples, the water content deduced from ATG/TG measurements (3.5 water molecules per structural formula) was overestimated [12]. Deduced formulae support the formation of rare-earth acid diphosphates according to the reaction

$$Na_4P_2O_7 + LnCl_3 + HCl + 3H_2O \rightarrow LnHP_2O_7 \cdot 3H_2O + 4NaCl.$$

The detection of IR POP modes at ∼950 and 750 cm^{-1} (Fig. 1) and NMR components near −20 ppm (Fig. 2) confirms the formation of diphosphates [17,18–20]. Taken into account splittings reported for ν_a(POP) and ν_s(POP) modes in other phosphates, POP groups of analyzed diphosphates must adopt a bended configuration [21].

On the other hand, the presence of a band at 3200 cm^{-1}, that does not disappear when water is eliminated, confirms the existence of OH groups [12]. Based on the lower antishielding effect of OH with respect to O*Ln* bonds in ^{31}P NMR signal, the component located at more positive chemical shift values has been assigned to OH-bearing tetrahedra, (PO_4H), and the second one to PO_4 tetrahedra. In MAS spectra, intensities of these components are near 1:1, which suggests that both signals correspond to two tetrahedra of the same diphosphate groups.

4.1. Structural features of diphosphates

In both diphosphates, rare-earth cations are bounded to six oxygens of four diphosphate groups. In La-diphosphate (structure type-I), three water molecules complete the La coordination, but in Er diphosphate (structure type-II), only two water molecules are bonded to Er cations. Differences in lanthanide coordination are due to different cation radii, that favors a lower coordination around smaller Er cations. In Figs. 3a and b, ORTEP drawings of the asymmetric units are given, including oxygens necessary to show the whole coordination of the rare-earth cations.

In both diphosphates, the unit cell contains two independent P tetrahedra connected by O(4) oxygens. According to data reported in other diphosphates, bridging P–O(4) bonds are appreciably longer than those located at external positions (1.61 and 1.52 Å,

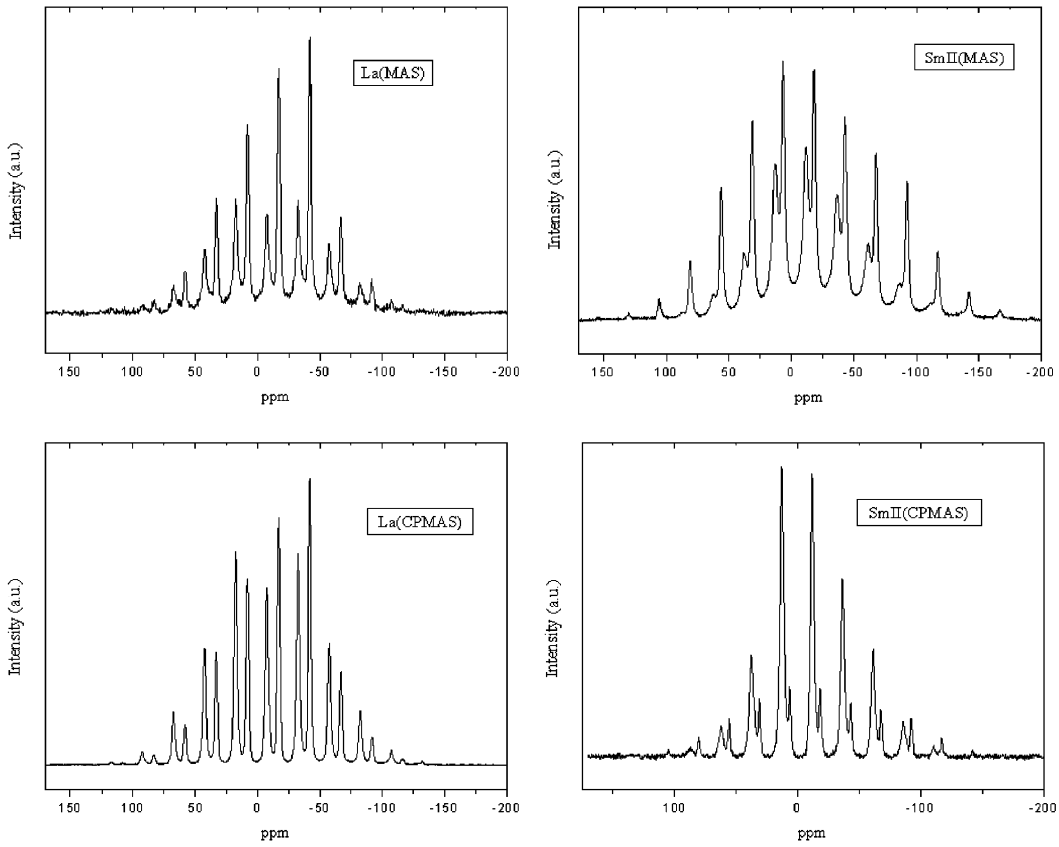

Fig. 2. ^{31}P MAS and CP-MAS NMR spectra of $Ln HP_2O_7 \cdot 3H_2O$ diphosphates, with Ln = La (type I) and Sm (type II). Components detected at decreasing chemical shifts correspond to PO_4H and PO_4 tetrahedra of diphosphate groups. In both cases, side-bands associated with the sample rotation are visualized.

respectively). P–O distances are similar in both compounds, but significant differences were detected on configuration of diphosphate groups. In the case of the La compound, diphosphate groups adopt a staggered (alternated) configuration, with three oxygens (O(1), O(5) and O(7)) of two tetrahedra bonded to La cations, in a tridentate mode. Torsion angles O1–P1–P2–O7, O2–P1–P2–O5 and O3–P1–P2–O6 are 38.7(5)°, 40.5(5)° and 51.1(9)°, respectively. For Er compound, diphosphate groups adopt a nearly eclipsed configuration, with torsion angles O2–P1–P2–O6, O3–P1–P2–O5 and O1–P1–P2–O7 equal to 13.7(3)°, 9.8(4)° and 17.4(3)°, in which, and only one oxygen of each tetrahedron is bonded to erbium cations (O(1) and O(7)). Due to the smaller size of the Er cations, the tridentate coordination is more difficult and the eclipsed configuration is adopted. As a consequence of these arrangements, the P–O–P angle is higher in Er diphosphate, 132.6(3)°, than in La diphosphate, 123.3(3)°. Differences on P–O–P angles explain differences observed on the splitting of ν_a(POP) and ν_s(POP) bands in IR spectra. An almost eclipsed configuration was also deduced in $GdHP_2O_7 \cdot 3H_2O$ [13], isostructural with $ErHP_2O_7 \cdot 3H_2O$, however in this dihosphate the P–O–P angle = 138.8° was considerably higher than that deduced in this work, P–O–P = 132.6(3)°.

The two analyzed diphosphates display a lamellar structure, in which edge-sharing lanthanide polyhedra are disposed forming chains along the *c*-axis in La diphosphate, and along the *b*-axis in Er diphosphate. These chains are joined together by diphosphate groups, to form structural planes of diphosphates (*ac* and *ab* planes, respectively). In both diphosphates, planes containing P–O–P triads are disposed almost perpendicular to lanthanide chains. In the first case, O(1), O(5) and O(7) oxygens of diphosphate groups are connected to one chain and O(6) to the contiguous one (Fig. 4a). In the second case, O(1) and O(7) are connected to the first chain and O(5) and O(6) to the adjacent one (Fig. 4b). The lamellar structure reported for $GdHP_2O_7 \cdot 3H_2O$ [13] is similar to that obtained here for $ErHP_2O_7 \cdot 3H_2O$ (type II), however, structure reported for $SmHP_2O_7 \cdot 4H_2O$ [14] is different to that obtained for $LaHP_2O_7 \cdot 3H_2O$ (type I). In this case, Sm cations share oxygens with four diphosphate groups but do not form chains with other Sm cations. In this diphosphate, a three-dimensional network is favored. From this fact, three Sm diphosphates can be formed: two displaying a

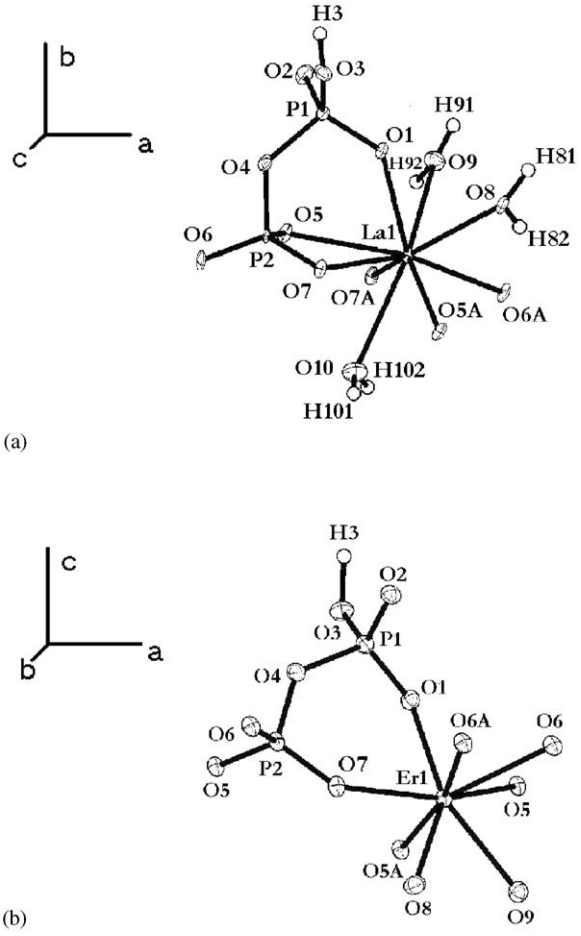

Fig. 3. ORTEP drawings of asymmetic units of $LaHP_2O_7 \cdot 3H_2O$ (a) and $ErHP_2O_7 \cdot 3H_2O$ compounds (b). Oxygens necessary to illustrate the *Ln* coordination are included.

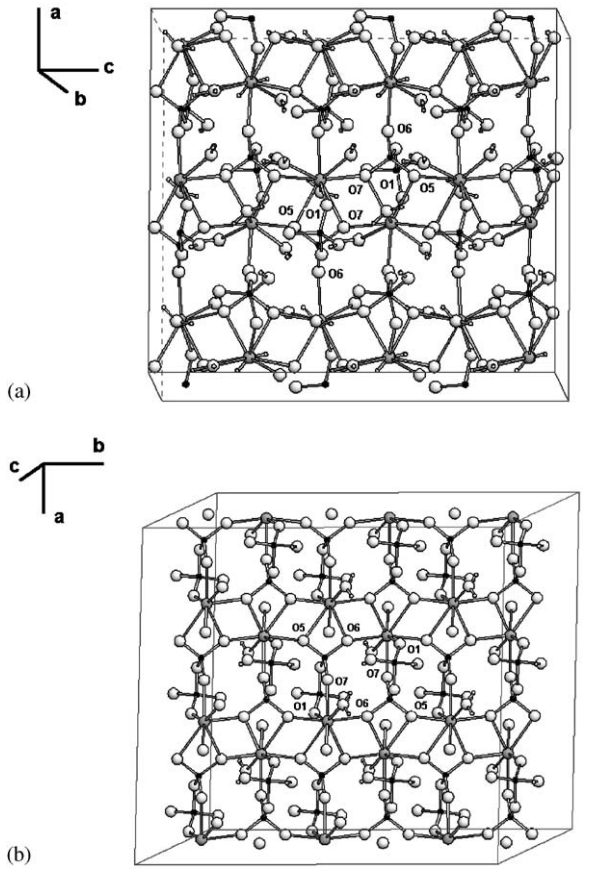

Fig. 4. Structural view of diphosphate layers of $LaHP_2O_7 \cdot 3H_2O$ (a) and $ErHP_2O_7 \cdot 3H_2O$. (b). Disposition adopted by diphosphate groups between adjacent lanthanum-chains is illustrated.

lamellar structure ($P\bar{1}$ and *Aba*2 symmetry) [12] and one displaying a three-dimensional network ($P2_1/n$ symmetry) [14].

At this point, it is interesting to analyze differences observed in NMR spectra of two layered diphosphates. The structural analysis showed that chemical environment of two tetrahedra are $P_1(OP)(OLn)(OH)(O)$ and $P_2(OP)(OLn)(OLnLn)_2$, which indicates that P_1 atoms are negatively charged with respect to P_2 atoms. This fact explain that chemical shift values of phosphorous coordinated to OH groups are more positive than those corresponding to the second tetrahedron. Moreover, differences on polarization strength of La and Sm cations explain that chemical shift values of Sm diphosphates (type-II) are appreciably lower (−11.8 and −18.3 ppm) than those of La diphosphate (type-I) (−7.6 and −16.9 ppm).

In both analyzed phosphates, P atoms occupy sites of low symmetry, which explain important asymmetry ($\eta = 0.7$ and 0.9), and anisotropy ($\Delta\sigma = 80$ and –115 ppm) values deduced from NMR spectra [12]. However, the analysis of NMR spectra shows that the sign of $\Delta\sigma$ is different in both diphosphates, indicating that atomic arrangement around P atoms is different in two compounds. However, the unique difference detected in two diphosphates is the relative disposition of two tetrahedra in diphosphate groups. In the case of the eclipsed configuration, interaction between oxygens of two tetrahedra is more important along the layer's perpendicular; however, this interaction decreases considerably when diphosphate groups adopt the alternated disposition. This fact explains differences observed on the $\Delta\sigma$'s sign resulting from the relative importance of chemical shit tensor values, along perpendicular and parallel directions to the layers.

In both types of compounds, only one tetrahedron of diphosphate groups is involved in formation of layer's planes, the second one pointing out of the layers. In this tetrahedron, one oxygen form part of P–O–P bridges, another is coordinated to rare-earth cations, and the two remaining ones are not involved in other coordinations. From this fact, protons of hydroxyl groups must be located in these oxygens, favoring the interaction with

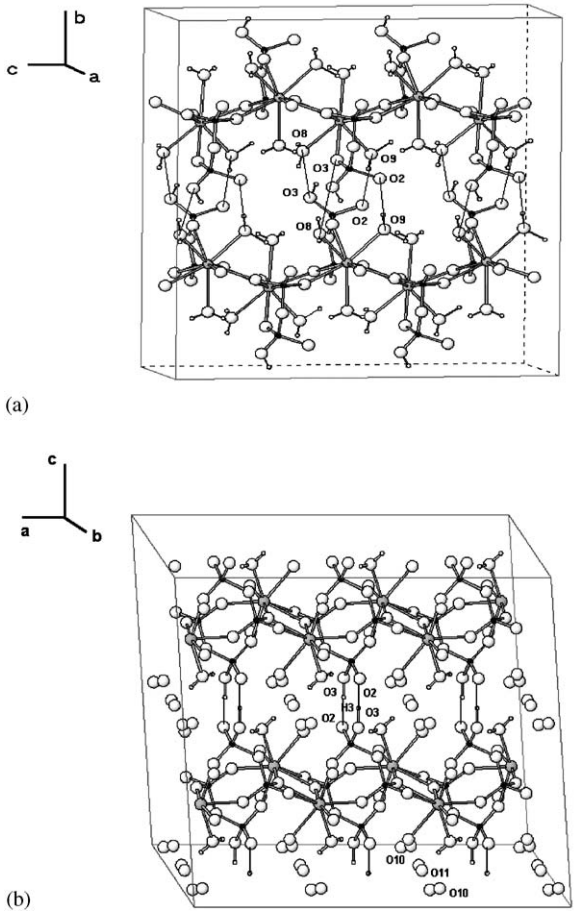

Fig. 5. Interlamellar spaces of diphosphates $LaHP_2O_7 \cdot 3H_2O$ (a) and $ErHP_2O_7 \cdot 3H_2O$ (b). Hydrogen bond interactions between contiguous layers are indicated.

adjacent layers (Fig. 5). In the case of La diphosphate, the interaction between OH groups and water molecules of adjacent layers (O(3)–O(8) and O(2)–O(9)) is favored ($OH–H_2O \sim 2.74/2.92$ Å). In the case of Er diphosphates, a symmetric interaction between PO_4H groups of contiguous layers (O(3)–O(2)) is produced ($OH–O_T \sim 2.57$ Å). This disposition favors open structures (6–7% by volume) in which water molecules, non coordinated to Er cations, are retained in two different crystallographic sites of the interlamellar space, O(10) and O(11) (1/2 occupation). In this compound, water–water interactions are also detected.

Structural features described, explain differences observed in IR spectra of two diphosphates. In La diphosphate, stretching modes of OH groups were detected at 3500–3600 cm^{-1}; however, in Er diphosphate these bands could not be differentiated from those of water. In this case, interaction between PO_4H groups of contiguous layers produce an important shift and broadening of OH bands, that impedes its detection. In La diphosphate, hydrogen bond interactions are smaller, confirming IR observations. This fact explains also the smaller cross-polarization detected between OH groups and P atoms in the La diphosphate with respect to that of the Sm (type II) diphosphate.

5. Conclusions

X-ray diffraction (XRD), IR and NMR (MAS and CP-MAS) techniques have been used to characterize acid $LnHP_2O_7 \cdot 3H_2O$ diphosphates, obtained by acid mixture of $Na_4P_2O_7$ and $LnCl_3$ solutions. Two structural environments, PO_4 and PO_4H, were identified by ^{31}P MAS-NMR spectroscopy. In two phosphates analyzed, a bended configuration for diphosphate groups was deduced from IR results.

The analysis of XRD patterns showed the existence of two structural forms, orthorhombic and triclinic, for analyzed diphosphates. Single-crystal X-ray determinations showed that in both cases layered structures are constituted by edge-sharing lanthanide polyhedra chains, joined together by diphosphate groups. Depending on rare-earth cation radius, the configuration of diphosphate groups changes from staggered (La diphosphate) to eclipsed (Er diphosphate). Differences on diphosphate group's configuration explains differences detected in chemical shift anisotropies in two ^{31}P MAS-NMR spectra of diphosphate compounds.

In both structures, OH groups are directed towards the interlamellar space, participating in hydrogen bond interactions between contiguous layers. In the first group, weak interactions between PO_4H groups and water molecules are produced; however, in the second group, strong interactions between PO_4H groups of contiguous layers are detected. Differences detected on hydrogen bond interactions explain some IR and NMR spectral features observed in two diphosphate types.

6. Supporting information

Data concerning atomic coordinates, distances and thermal factors of $LaHP_2O_7 \cdot 3H_2O$ and $ErHP_2O_7 \cdot 3H_2O$ diphosphates are available at deposited files. Further details of the crystal structure investigations can be obtained from the Fachinformationszentrum Karlsruhe, 76344 Eggenstein-Leopoldshafen, Germany, (fax: +49-7247-808-666; mail to: crysdata@fiz.karlsruhe.de) on quoting the depositary numbers CSD 413831 and 413832.

Acknowledgments

S.B.M. thanks the Instituto de Cooperación Hispano-Arabe for a graduate fellowship. We thank I. Sobrados

and R. Rojas for NMR and ATD/TG technical assistance.

References

[1] A. Clearfield, J.A. Stynes, J. Inorg. Nucl. Chem. 26 (1964) 117.
[2] G. Alberti, in: P.A. Williams, M.J. Hudson (Eds.), Recent Developments in Ion Exchange, Elsevier Applied Science, London, 1987.
[3] M.B. Dines, P.M. Digiacomo, K.P. Callahan, P.C. Griffith, R.H. Lane, R.E. Cooksey, in: J.S. Miller (Ed.), Chemically Modified Surfaces in Catalysis and Electrocatalysis, ACS Symposium Series, Vol. 192, Washington, DC, 1982.
[4] D.J. MacLachlan, K.R. Morgan, J. Phys. Chem. 94 (1990) 7656.
[5] A. Clearfield, Annu. Rev. Mater. Sci. 14 (1984) 203.
[6] N.J. Clayden, J. Che. Soc. Dalton Trans. (1987) 1877.
[7] J. Sanz, J.E. Iglesias, J. Soria, E.R. Losilla, M.A.G. Aranda, S. Bruque, Chem. Mater. 9 (1997) 996.
[8] V. Korthuis, N. Khosrovani, A.W. Sleight, N. Roberts, R. Dupree, W.W. Warren, Chem. Mater. 7 (1995) 412.
[9] M. Kizilyalli, J. Less-Commun. Mater. 127 (1987) 147.
[10] Y.V. Tananaev, V.G. Kuznetsov, V.P. Vasil'eva, Inorg. Mater. 3 (1967) 87.
[11] E.G. Afonin, N.I. Pechurova, Russ. J. Inorg. Chem. 35 (1990) 783.
[12] S. Ben Moussa, I. Sobrados, J.E. Iglesias, M. Trabelsi-Ayedi, J. Sanz, J. Mater. Chem. 10 (2000) 1973.
[13] F. Chehimi-Moumen, D. Ben Hassen-Chehimi, M. Ferid, M. Trabelsi-Ayadi, Mater. Res. Bull. 36 (2001) 365.
[14] F. Chehimi-Moumen, M. Ferid, D. Ben Hassen-Chehimi, M. Trabelsi-Ayadi, Solid State Sci. 4 (2002) 979.
[15] S. Ben Moussa, Doctoral Thesis, University of Autónoma, Madrid, 2000.
[16] Bruker WINFIT Program, Bruker Rep. 140 (1994) 43.
[17] N.N. Chudinova, G.M. Balagina, L.P. Shklover, Izv. Akad. Nauk SSSR Neorg. Mater. 13 (1977) 2075.
[18] L. Griffiths, A. Root, R.K. Harris, K.J. Parker, A.M. Chippendale, F.R. Tromans, J. Chem. Soc. Dalton Trans. (1986) 2247.
[19] A. Cheetham, N.J. Clayden, C.M. Dobson, R.J.B. Jakeman, J. Chem. Soc. Commun. (1986) 194.
[20] S. Prabhakar, K.J. Rao, C.N.R. Rao, Chem. Phys. Lett. 139 (1987) 96.
[21] M. Harcharras, A. Ennaciri, A. Rulmont, B. Gilbert, Spectrochim. Acta 53 (1997) 345.